

Polyvinyl Butyral-Based Thin Film Polymeric Electrolyte for Dye-Sensitized Solar Cell with Long-Term Stability

Kuei-Fu Chen*, Chien-Hung Liu, Hsin-Kai Huang, Chun-Hung Tsai, Fu-Rong Chen

Department of Engineering and System Science, National Tsing-Hua University, Hsinchu City, 30013, Taiwan (ROC)

*E-mail: g9711512@oz.nthu.edu.tw

Received: 1 February 2013 / Accepted: 23 February 2013 / Published: 1 March 2013

Polyvinyl butyral (PVB), a polymer used world-wide in laminated glass, has been incorporated into dye-sensitized solar cells (DSSCs) as a quasi-solid polymeric electrolyte (SPE) thin film. SPE thin films soaked with different amounts of liquid electrolyte were prepared. The surface morphologies, the diffusion coefficients, and the ionic conductivities of the SPE thin films were analyzed as a function of the liquid electrolyte content (in weight percent). The optimal ionic conductivity was measured to be approximately 1.1×10^{-3} S/cm, which is approximately six orders of magnitude higher than that of the original PVB thin film. The effective resistance of DSSC devices incorporating these thin films was measured using electrochemical impedance spectroscopy (EIS). The EIS spectra show a unique pattern consisting of four semi-circles, which is different from the three-semi-circle pattern observed for DSSCs with a liquid electrolyte. The SPE devices exhibited a high conversion efficiency of 5.46% at 100 mW/cm^2 , approximately 94% that of corresponding liquid-electrolyte cells. The devices' long-term durability was tested to be over 3000 hrs.

Keywords: dssc, long-term, electrolyte, PVB

1. INTRODUCTION

Over the past decade, after a breakthrough made by Gratzel and co-workers in 1991[1], liquid-electrolyte-based dye-sensitized solar cells (DSSCs) composed of films of porous metal oxide nanoparticles such as ZnO and TiO₂ have attracted widespread interest in science and technology. DSSCs are classified as a third-generation photovoltaic (PV) technology that provides the following advantages over other photovoltaic technologies: low production cost, simple fabrication procedure, and reasonable conversion energy [2.3.4]. The highest reported solar conversion rate of liquid-state DSSCs is 13% [5]. Although this conversion efficiency is currently still lower than that of classical

crystalline silicon cells, there is great potential for improvement toward the theoretical efficiency of 21% [6].

The main challenge facing liquid-electrolyte-based DSSCs is the leakage and the valorization of the organic solvent limiting the long-term durability and the practical use of DSSC [7, 8, 9]. Therefore, the solidification of the electrolytes used in these devices has been one of the most crucial research directions in the field of DSSCs. Many groups have focused on the substitution of the liquid electrolyte with a solid or gel electrolyte [10-22].

Hole transport materials (HTMs) [10, 11, 12, 13] are often used as solid-state electrolytes for DSSCs. There are inorganic HTMs such as CuI [10] and CuSCN [11] and organic HTMs such as Spiro-OMeTAD [12, 13] that are widely used in solid-state DSSCs. However, because of their low power conversion efficiencies due to their poor penetration of nanoporous TiO₂ films, HTMs cannot satisfy the requirements for DSSC applications. Polymer “gel” electrolytes (PGEs) have attracted attention for their application in energy storage or conversion devices such as fuel cells [14], Li batteries [15, 16] and DSSCs [17-22]. The most frequently used polymers in PGEs are poly(ethylene oxide) (PEO) [17, 18], poly(vinylidene fluoride-co-hexafluoropropylene) (PVDF-HFP) [19, 20], poly(methyl methacrylate) (PMMA) [21] and polyvinyl alcohol (PVA) [22]. Due to their instability, PGEs still face some technological challenges, such as the crystallization of iodine, phase separation and, most importantly, the strict sealing procedures required to fabricate DSSCs with good long-term stability.

In this research, we used PVB as a host polymer to create a PVB-based quasi-solid polymeric electrolyte (PVB-SPE) for DSSCs through the following steps. PVB films were first fabricated by mixing PVB powders and a plasticizer using a Brabender mixer. The product was then hot pressed into films. The PVB films were soaked in a liquid electrolyte to make them ionically conductive. The PVB-SPE films behaved like sponges, retaining a large amount of the liquid electrolyte after soaking, but they still remained solid, as shown in Fig. 1. These PVB-SPE films have three advantages:

(1) They makes the sealing procedure required for the fabrication of DSSC devices much easier and yield better long-term stability by leaking low amounts of the liquid electrolyte.

(2) During the assembly process, the electrolyte inside the PVB-SPE films can be easily squeezed onto a porous TiO₂ electrode, comparable to the “gel” electrolyte in PGEs.

(3) The electrolyte in TiO₂ electrodes can be protected from evaporation by capping with PVB-SPE films.

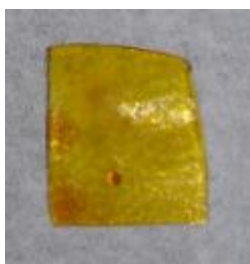


Figure 1. The picture of PVB-SPE thin film

The most important reason why we chose polyvinyl butyral (PVB) as the host polymer is that PVB has been used in laminated safety glass for over 60 years due to its high stability against sunlight, without degradation in its transparency or adhesion to glass. The implementation of an ionically conductive PVB film as a solid-state electrolyte film for electrochromic devices (ECDs) have been reported [23]. Thus, it is believed that PVB-SPE may provide a way to link DSSC devices with ECD energy-saving smart windows in the architecture and automotive sectors in the future.

In this paper, we report that the efficiency of solid-state DSSCs fabricated with PVB-SPE was measured to be approximately 5.46%, which is approximately 94% that of corresponding liquid-state devices. We believe that this efficiency can be further optimized in the future. The lifetime of these devices is currently over 3000 hours.

2. EXPERIMENTAL SECTION

2.1. Preparation of TiO_2 working electrode

A fluorine-doped SnO_2 conducting glass substrate (FTO, 8-10 Ω/sq , 2.2 mm in thickness, Pilkington TEC glass) was first cleaned with DI water, acetone, and IPA (isopropyl alcohol), sequentially. The photoelectrode was then soaked in a 0.04 M TiCl_4 aqueous solution at 70°C for 30 minutes. A TiO_2 paste was prepared independently from the anatase TiO_2 nanoparticles using the sol-gel method. A TiO_2 thin film measuring 15 μm in thickness was coated on the treated photoelectrode by screen printing the prepared TiO_2 paste. The TiO_2 -coated working electrode was then gradually heated to 500 °C in ambient air for 50 minutes, then cooled slowly to room temperature. The active area of the TiO_2 -coated photoelectrode was circular with a diameter of 6 mm. After sintering, the TiO_2 -coated photoelectrodes were immersed in a solution of 5×10^{-4} M cis bis(isothiocyanato) bis-(2,2'-bipyridyl-4-4'-dicarboxylato)-ruthenium(II) bis-tetrabutylammonium (Solaronix, N719) in acetonitrile and tert-butanol (volume ratio of 1:1) at room temperature for 24 hours. After dye adsorption, the TiO_2 -coated photoelectrodes were then rinsed with ethanol to remove the remaining dye.

2.2. Preparation of PVB-SPE

We used two different types of electrolytes to fabricate PVB-SPE. Type I was an organic solvent mixture of GBL and NMP with a volume ratio of 7:3. GBL and NMP contain 0.5 M LiI and 0.1 M I_2 , respectively. Type II was a MPN-based electrolyte composed of a mixture of 0.5 M DMPII, 0.1 M LiI and 0.05 M I_2 . PVB-SPE films were made by immersing the PVB thin films in the type I and II electrolytes for 10, 20, 30, 40, 50 and 60 minutes.

The ionic conductivity of PVB-SPE films depends on the immersion time. After immersion, the PVB-SPE thin films were fixed between two mirror-polished stainless steel rod-shaped electrodes (diameter = 12 mm), and the ionic conductivity was measured and calculated using the following formula:

$$\sigma = \frac{L}{A \times R_s} \tag{1}$$

where L is the distance between the TiO₂-coated working electrode and the Pt counter electrode and A is the surface area of the TiO₂ on the working electrode. The ohmic serial resistance (R_s) was determined from a Nyquist plot obtained by measuring the impedance at room temperature.

2.3. Preparation of PVB-SPE and LSE-based DSSC devices

To quantitatively compare the efficiency and durability of solid-state electrolyte-based DSSCs, in this study, DSSC devices were fabricated with both PVB-SPE electrolytes and the corresponding type I and type II liquid-state electrolytes (LSE). A 60-μm-thick hot-melted spacer (Dopont, Surlyn) was placed on the dye-adsorbed TiO₂-coated working electrode, and the electrode was then assembled with a counter electrode created by dropping a H₂PtCl₆ isopropanol solution onto a FTO glass substrate annealed at 450°C for 20 minutes.

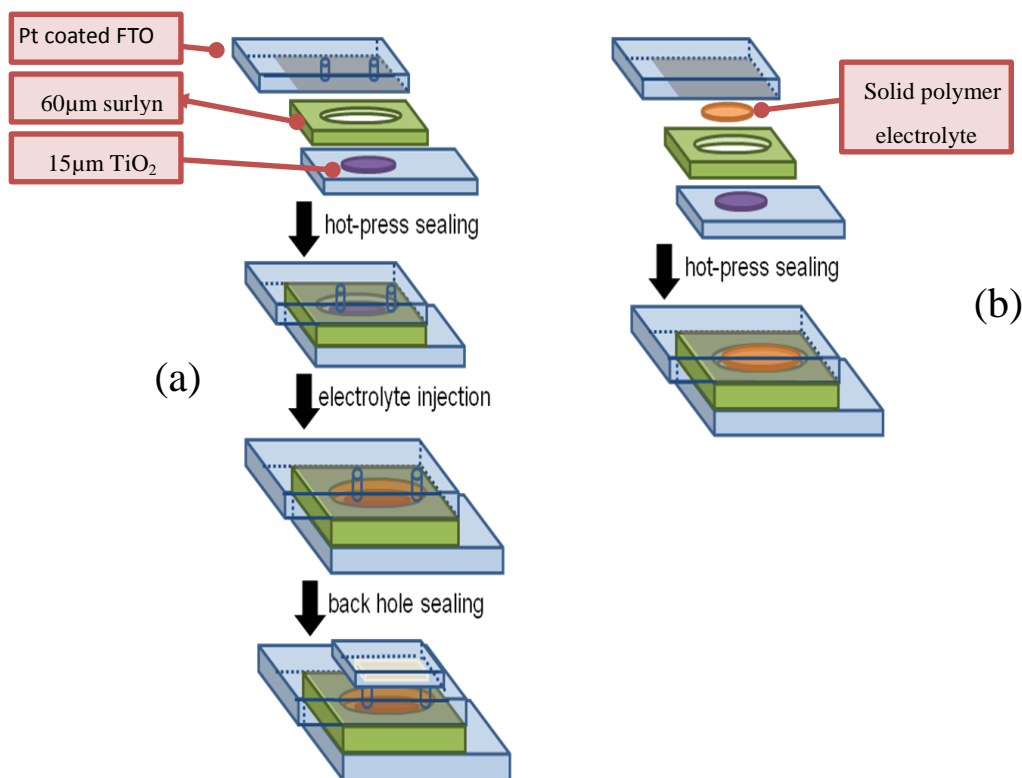


Figure 2. (a) The fabrication process of LSE-DSSC. 2(b) The fabrication process of PVB-SPE-DSSC

The LSE-based DSSC device was fabricated by drilling two holes on the counter electrode before the liquid electrolyte was injected into the cell. Meanwhile, the PVB-SPE-based DSSC device was simply fabricated by placing the PVB-SPE film over the dye-absorbed TiO₂ film; the device was then sealed by hot pressing under a pressure of 80 psi at 130 °C. The sealing procedures for the liquid-state and the quasi-solid-state electrolyte-based DSSCs are shown in Fig. 2. Both the SPE- and LSE-based DSSC were illuminated by a class-A quality solar simulator with a light intensity of 100 mWcm⁻²

² (AM1.5), which was calibrated with a standard silicon cell. The photocurrent-voltage curves of all of the DSSCs were obtained using an electrochemical analyzer (Autolab, PGSTAT30). The electron transport process in the cells was evaluated using electrochemical impedance spectroscopy (EIS).

3. RESULTS AND DISCUSSION

3.1 The Absorbance of PVB-SPE film

The properties of SPE-based DSSC devices strongly depend on the amount of liquid electrolyte absorbed. The liquid absorbance (A_b) of a PVB-SPE film was defined as

$$A_b = \frac{w - w_0}{w_0} \quad (2)$$

where W_0 and W are the total weight of the PVB-SPE film before and after immersion, respectively. Fig. 3 shows the absorbance of the films in the type I and II electrolytes as a function of time. The absorbance increases with the immersion time for both types of electrolytes. The absorbance reaches maximum values of 0.95 and 0.48 for the type I and II electrolytes, respectively, in approximately 60 minutes. As a result, for the same immersion time, the PVB film absorbs more type I electrolyte than type II electrolyte.

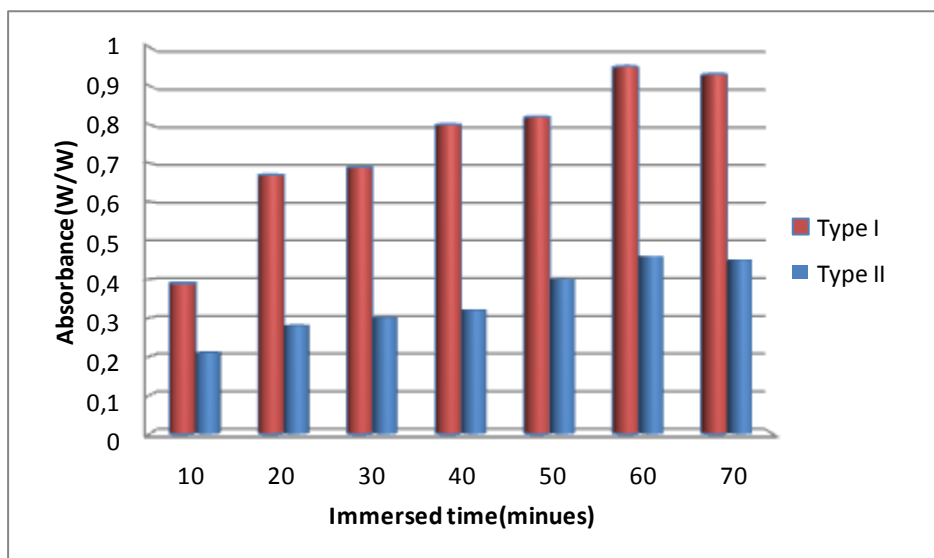


Figure 3. Absorbance of PVB as a function of time for type I and II electrolytes

3.2. The surface morphology and chemical analysis of PVB-SPE film

The surface morphology of the PVB thin films was also strongly influenced by the amount of electrolyte absorbed and thus the immersion time. Fig. 4 (a) shows the surface morphology of an as-

received PVB thin film at a magnification of 2,000x. It shows a rough surface without any pores. The surface morphology was modified as the PVB film was immersed in the type I (Fig. 4(b) and (c)) and II (Fig. 4(d) and (e)) electrolytes for 10 and 60 minutes, respectively. After the PVB thin film absorbed the type I or type II electrolyte, iodine could be detected on the film's surface, as shown in Fig. 4(b) to (e). In fact, PVB can be dissolved in GBL.

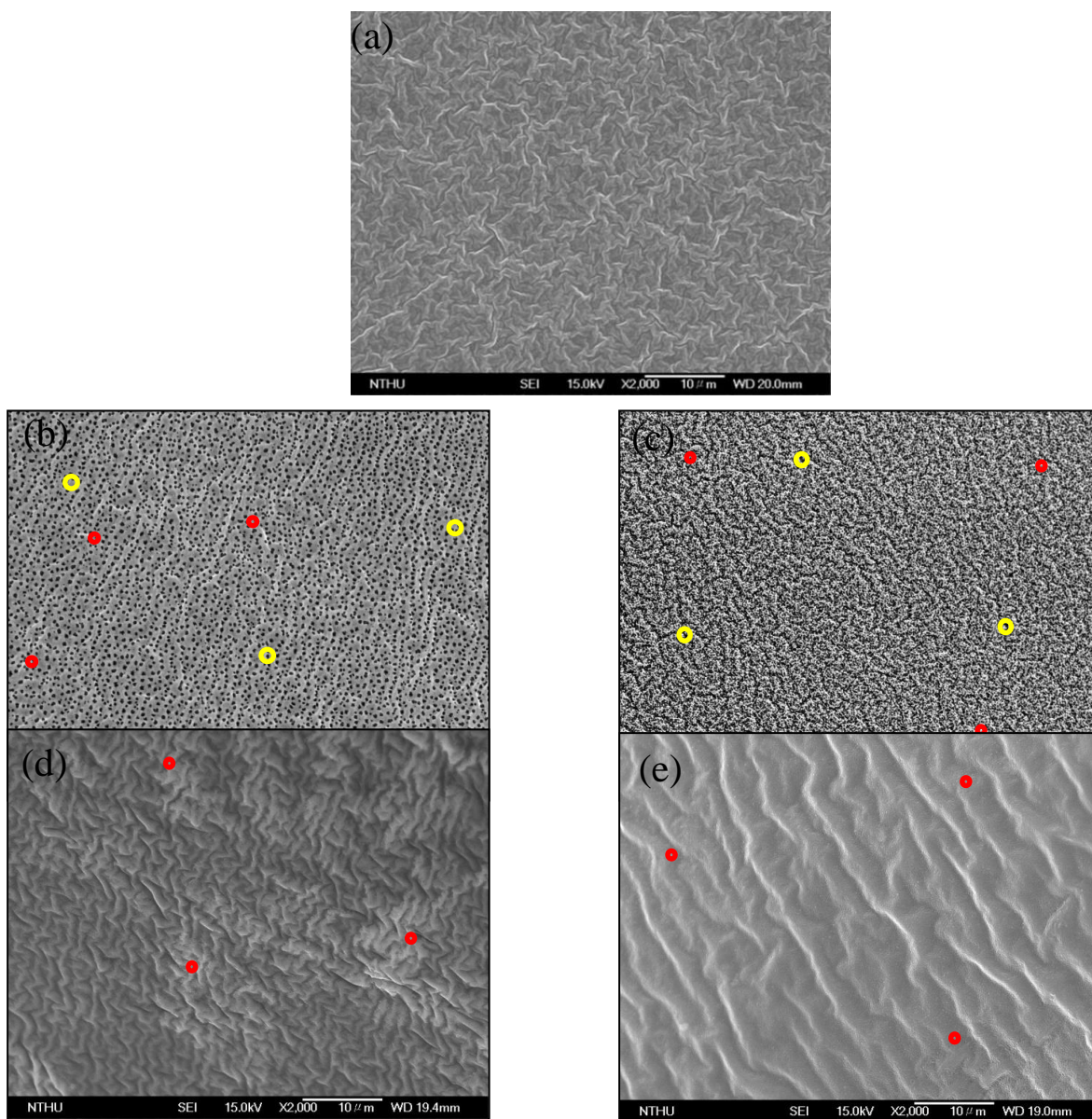


Figure 4. (a) show the surface morphology of as-received PVB thin film at 2,000X (b) the surface morphology of PVB thin film after immersed in type I based electrolyte for 10 minutes. (c) the morphology of PVB thin film immersed in type I based electrolyte for 60 minutes. Typical porous structures are highlighted with yellow circles in the (b) and (c). (d) the surface morphology of PVB thin film immersed in type II based electrolyte for 10 minutes (e) the surface morphology of PVB thin film immersed in type II based electrolyte for 60 minutes. The EDX spectra are taken from the positions of red circles, where show brighter contrast in (b), (c), (d) and (e).

As a result, a porous structure, as indicated by yellow circles in Fig. 4(b) and (c), was observed on the surface after immersion in the type I PVB-SPE electrolyte. The pores in the type I PVB film are called a sub-phase and contain a mixture of dissolved PVB and type I electrolyte. It was also found that the pore size increases with the immersion time, as shown in Fig. 4(b) and (c). However, pores were not clearly observed after immersion in the type II electrolyte, as shown in Fig. 4(d) and (e).

Because the sub-phase (pores in the SPE film) contains more electrolyte, it is believed that the sub-phase may offer faster ion-conducting channels. It can be expected that the ionic conductivity of the type I PVB-SPE is higher than that of the type II PVB-SPE. The bright spots indicated by red circles on the surface of both the type I and II PVB-SPE films are iodine-rich areas. This was confirmed by the EDX spectra. Fig. 5(a), (b) and (c) show the EDX spectra of an as-received and type I and type II PVB-SPE films, respectively.

The gold signal in the EDX spectrum is due to gilding, which improves the conductivity of PVB thin films such that they can be observed without charging by SEM. The spectra of the type I and II PVB-SPE films show the same carbon and oxygen peaks as those of the as-received PVB; in addition, peaks at approximately 3.942 keV and 4.2 keV corresponding to the L-peaks of iodine are observed.

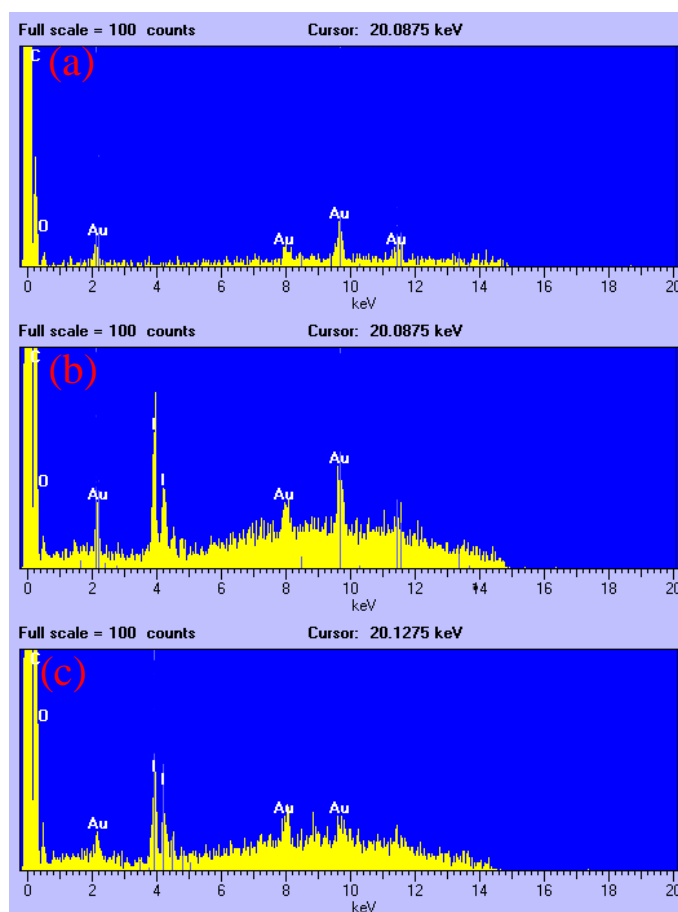


Figure 5. (a) EDX spectrum from as-received PVB thin film, (b) EDX spectrum recorded from red circled positions of Fig. 4(b) and (c) for type I PVB-SPE thin film. (c) EDX spectrum recorded from red circled positions of Fig. 4(d) and (e) for type II PVB-SPE thin film

These results indicate the type I and type II PVB-SPE thin films were full of iodine ions, which contributed to the ionic conductivity of the PVB-SPE thin films.

Fig. 6 shows that the sub-phase plays an important role in the ionic conductivity of the PVB-SPE films used in the DSSC devices. The reasons for this are as follows. (1) As shown in Fig. 6(a), local solvent channels for ion conduction can be established by the sub-phase, which play a major role in supporting the ion conductivity of the polymer electrolyte, in our case, the ionic-PVB thin film. (2) As shown in Fig. 6(b), the liquid-like sub-phases can penetrate the porous structure of the TiO_2 nanoparticle layer, which enhances the re-generation rate of dye on the TiO_2 surface.

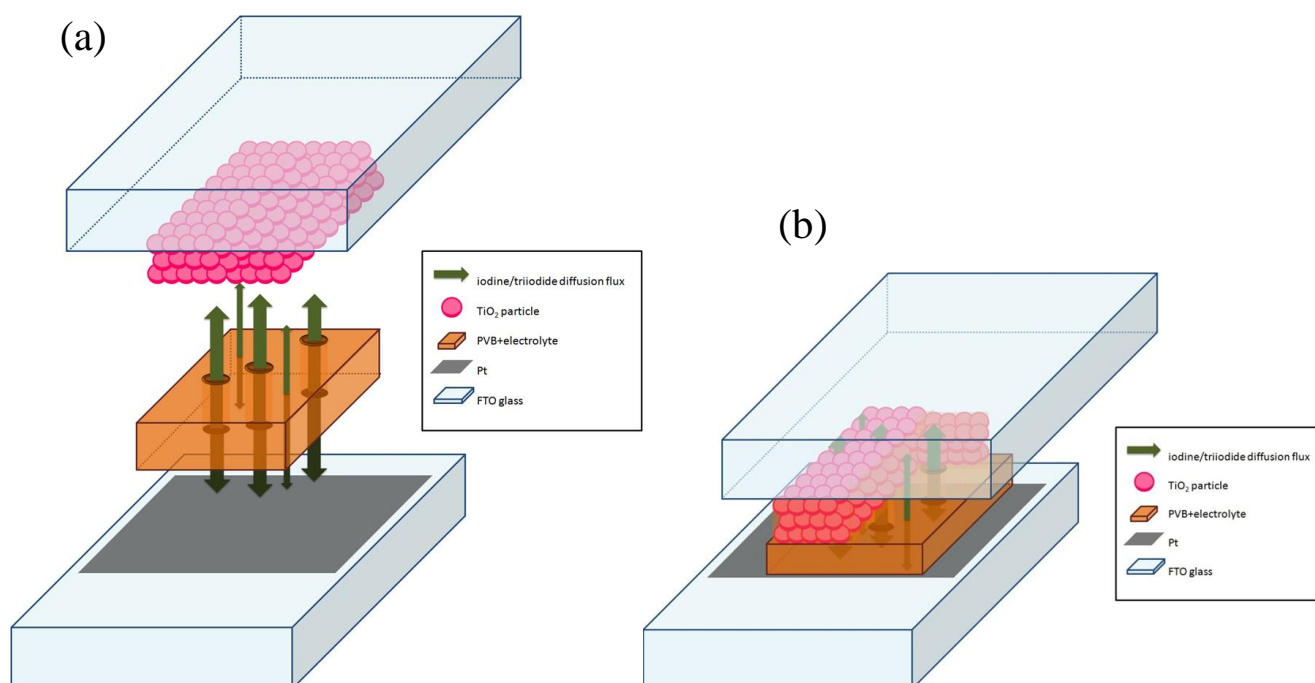


Figure 6. (a) the local ion channel is formed by the dissolved PVB and the liquid electrolyte soaked by PVB film. In the ion channel, it is gel-like electrolyte which is less viscous than elsewhere in the rest of the PVB film. The ion channel offers better diffusion path for I^-/I_3^- and ion conductivity. The size of the green arrows means the diffusion flux of I^-/I_3^- . 6(b) Being squeezed in the hot-press process, the sub-phase will penetrate into the porous structure of TiO_2 nanoparticle layer due to its better fluidity. The brown color covering the entire TiO_2 range in the figure demonstrates this phenomenon. The better penetration rate enhances the re-generation rate of dye on TiO_2 surface.

3.3. The diffusion coefficient and ionic conductivity of ionic PVB thin films

The efficient transport of iodine and tri-iodine ions in the electrolyte is an essential requirement to guarantee the high performance of DSSC devices because the oxidized state of the dye (dye^+) must be regenerated efficiently by I^- ions after electrons from the excited state of the dye (dye^*) are injected into the conduction band of TiO_2 . If the transport of iodine and tri-iodine ions is not efficient enough, the electrons in the conduction band of TiO_2 will recombine with the tri-iodine ions in the electrolyte,

leading to a reduction in the electron current produced in the DSSC system.

To study the ionic conduction properties of the PVB-SPE film, the diffusion coefficient of the I_3^- ions in a PVB-SPE film was measured first. Although the diffusion coefficients of the diffusing species I^- and I_3^- are on the same order of magnitude, it is believed that the tri-iodine is the diffusion-limiting species because I_3^- is heavier and the concentration of I_3^- is lower than that of I^- in the redox reaction. The diffusion coefficient of tri-iodine ($D_{I_3^-}$) in the PVB-SPE film was evaluated at a diffusion-limited current density within an electrochemical cell prepared by sandwiching the PVB-SPE film between two Pt-coated FTO electrodes. The diffusion-limited current density was determined by cycle voltammetry using a slow scan rate of 10 mV/s. The diffusion coefficient of I_3^- in the PVB-SPE thin film was proportional to the diffusion current density given by the following equation [24]:

$$J = \frac{2nFC D}{l} \quad (3)$$

where n is the number of electrons involved in the electrode reaction, F is the Faraday constant, C is the initial concentration of tri-iodine ions and l is the distance between two electrodes. The diffusion coefficients were determined to be approximately $4.8 \times 10^{-6} \text{ cm}^2 \text{ s}^{-1}$ and $4.1 \times 10^{-6} \text{ cm}^2 \text{ s}^{-1}$ for the type I LSE and PVB-SPE systems, respectively. Additionally, the diffusion coefficients for the type II LSE and PVB-SPE systems were determined to be approximately $7.6 \times 10^{-6} \text{ cm}^2 \text{ s}^{-1}$ and $6.6 \times 10^{-7} \text{ cm}^2 \text{ s}^{-1}$, respectively. Because PVB cannot be completely dissolved in the type II electrolyte (MPN), the diffusion coefficient of I_3^- in the type II PVB-SPE system is the lowest. In general, Table 1 shows that the diffusion coefficient of I_3^- in type II LSE is the highest and lower in both quasi-solid systems. Interestingly, it is evident that the diffusion coefficient of I_3^- in type I PVB-SPE is higher than that in type II PVB-SPE. This strongly supports the notion that the sub-phase plays an important role in providing ionic channels in the SPE electrolyte, as shown in Fig. 6.

Table 1. The measured diffusion coefficient for Type I and Type II PVB-SPE electrolytes

| electrolyte | Diffusion coefficient |
|-----------------|--|
| Type I LSE | $4.8 \times 10^{-6} \text{ cm}^2 \text{ s}^{-1}$ |
| Type I PVB-SPE | $4.1 \times 10^{-6} \text{ cm}^2 \text{ s}^{-1}$ |
| Type II LSE | $7.6 \times 10^{-6} \text{ cm}^2 \text{ s}^{-1}$ |
| Type II PVB-SPE | $6.6 \times 10^{-7} \text{ cm}^2 \text{ s}^{-1}$ |

The relationship between immersion time and the ionic conductivity of the PVB-SPE film is shown in Fig. 7. The figure shows that longer immersion times yield PVB-SPE films with higher ionic conductivity for both the type 1 and II electrolytes. However, the ionic conductivity reaches its optimum values of $1.1 \times 10^{-3} \text{ S/cm}$, in the type II PVB-SPE film and $4.7 \times 10^{-5} \text{ S/cm}$ in the type I PVB-SPE film after 60 minutes of immersion. This result is in very good agreement with the absorbency

results shown in Fig. 3. This indicates that the absorbance is a key parameter related to ionic conductivity.

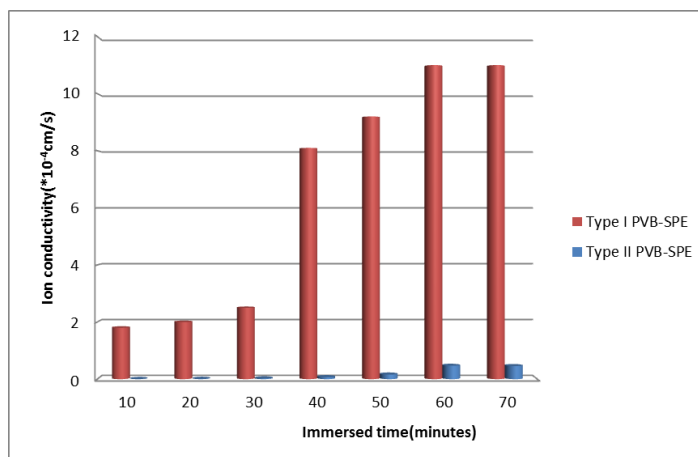


Figure 7. the relationship of the ion conductivity of PVB-SPE with immersion time in type I and type II electrolytes

3.4. The performance and electrochemical characteristic of the cell

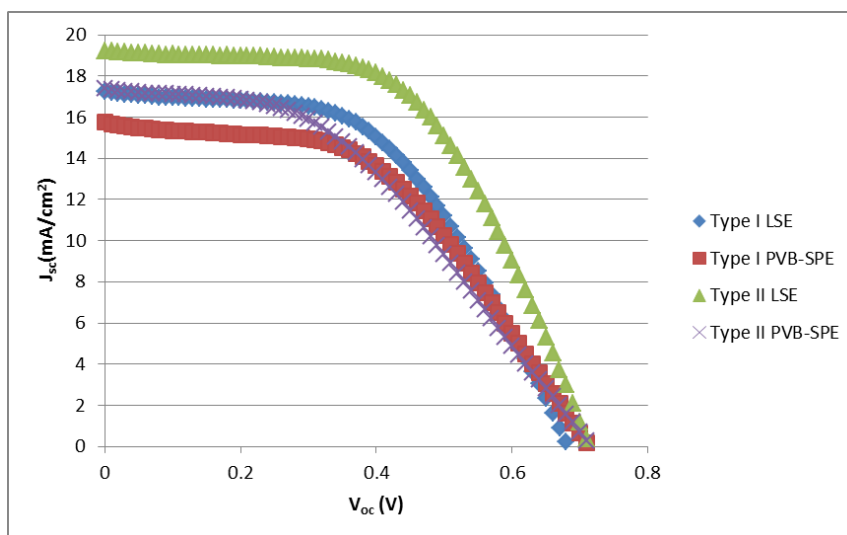


Figure 8. the J-V curve of the DSSCs with four different electrolytes type I LSE (GBL+NMP, liquid), type II LSE (MPN, liquid), type I PVB-SPE (GBL+NMP+PVB, quasi-solid) and type II PVB-SPE (MPN+PVB, quasi-solid)

Fig. 8 shows the J-V characteristics of DSSCs fabricated with four different electrolytes: type I LSE (GBL+NMP, liquid), type II LSE (MPN, liquid), type I PVB-SPE (GBL+NMP+PVB, quasi-solid) and type II PVB-SPE (MPN+PVB, quasi-solid). The corresponding open-circuit voltage (V_{oc}), short-circuit current density (J_{sc}), fill factor (FF), and total energy conversion efficiency (η) of these cells are given in Table 2. The energy conversion efficiencies of the type I and II LSE (liquid electrolyte)-based

DSSCs are 5.84% and 7.69%, respectively, while the efficiencies of the type I and II PVB-SPE (quasi-solid state electrolyte)-based DSSCs are 5.46% and 5.33%, respectively. It is worth noting that the efficiencies of the SPE type are 94% and 69% of the efficiency of their corresponding liquid cells.

Table 2. The J-V data of the DSSCs with four different electrolytes type I LSE (GBL+NMP, liquid), type II LSE (MPN, liquid), type I PVB-SPE (GBL+NMP+PVB, quasi-solid) and type II PVB-SPE (MPN+PVB, quasi-solid). V_{oc} (V): open-circuit voltage, J_{sc} (mA/cm²): short-circuit current density, FF: fill factor, and η (%): total energy conversion efficiency of these cells

| | Type1 LSE | Type I PVB-SPE | Type II LSE | Type II PVB-SPE |
|----------|-----------|----------------|-------------|-----------------|
| J_{sc} | 16.21 | 15.59 | 19.23 | 17.42 |
| V_{oc} | 0.67 | 0.71 | 0.71 | 0.72 |
| FF | 0.54 | 0.49 | 0.56 | 0.43 |
| η | 5.84 | 5.46 | 7.69 | 5.33 |

In this study, it was evident that the PVB-SPE-based DSSCs showed lower J_{sc} and higher V_{oc} than those based on liquid electrolyte systems. It is easy to understand that the lower J_{sc} value is caused by the hindrance of ionic movement in the PVB-SPE thin films. The V_{oc} value of DSSC devices is given by equation 4. [25]

$$V_{oc} = \left[\frac{kT}{e} \right] \ln \left\{ \frac{I_{inj}}{n_{cb} k_{et} [I_3^-]} \right\} \quad (4)$$

where k is the Boltzmann constant, T is absolute temperature, e is charge of a single electron, I_{inj} is the charge flux due to sensitized injection, n_{cb} is the concentration of electrons on the surface of TiO_2 nanoparticles, k_{et} is the reaction rate constant of the I_3^- dark reaction on TiO_2 , and $[I_3^-]$ is the concentration of I_3^- in the electrolyte. In the PVB-SPE-based DSSCs, the interface between the surface of the TiO_2 electrode and the PVB-SPE polymer is highly resistant (as will be shown later) to ionic conductivity, which suppresses electron transfer from TiO_2 back to I_3^- ; in other words, the reaction rate constant of the I_3^- back reaction decreases. From equation [4], the high interfacial resistance in the solid-state cell increases the value of V_{oc} .

Electrochemical impedance spectroscopy (EIS) was used to study the internal resistances and the charge-transfer kinetics of the DSSCs. The results are shown in Fig. 9. In general, the EIS spectrum of liquid-electrolyte-based DSSCs exhibits three semi-circles, which are associated with the interfacial resistances and the oxidation-reduction reaction in DSSCs. These three interfacial resistances are related to the electrochemical reaction at the Pt/ electrolyte interface (R_{ct1}), the charge-transfer process that occurs at the TiO_2 /dye/electrolyte interface (R_{ct2}) [26], and the Warburg diffusion of I_3^-/I^- in the electrolyte (R_{diff}) [26].

In this study, R_{ct1} was not clearly observed but overlapped with R_{ct2} , which implies that the Pt electrodes exhibited a good redox ability in the devices. The R_{ct2} of the PVB-SPE cells was larger than

that of the corresponding liquid state (LSE) cells. This is because PVB-SPE films are more viscous, which gives rise to a higher resistance to electron transport.

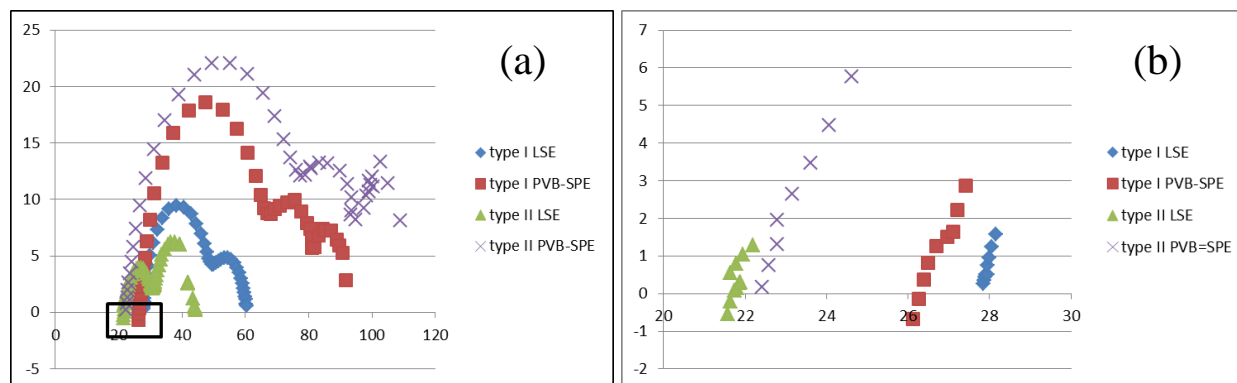


Figure 9. (a) the EIS curves of the DSSCs with four different electrolytes type I LSE (GBL+NMP, liquid), type II LSE (MPN, liquid), type I PVB-SPE (GBL+NMP+PVB, quasi-solid) and type II PVB-SPE (MPN+PVB, quasi-solid). (b) the first semi-circle in EIS spectrum for DSSC with four different electrolytes type I LSE (GBL+NMP, liquid), type II LSE (MPN, liquid), type I PVB-SPE (GBL+NMP+PVB, quasi-solid) and type II PVB-SPE (MPN+PVB, quasi-solid)

As the charge-transfer resistance of the $\text{TiO}_2/\text{dye}/\text{electrolyte}$ interface (R_{ct2}) rises, the electrons in the TiO_2 conduction band do not easily re-enter the reaction with I_3^- in the electrolyte. This result is in agreement with the above discussion, and yields a higher V_{oc} in devices featuring PVB-SPE films. For the same reason, the R_{ct3} of the PVB-SPE cells was also higher than that of the corresponding liquid-state cells, i.e., because ion conduction becomes more difficult in the PVB-SPE film. Additionally, as the Warburg diffusion of I_3^-/I^- in the electrolyte (R_{diff}) rises, the diffusion coefficient and the ionic conductivity decrease, which is in agreement with the above discussion on what generates a lower J_{sc} in devices with PVB-SPE films.

The most important finding is that the Nyquist plot of the PVB-SPE-based cells (Fig. 9) shows an extra semicircle in the lower-frequency region, which has not yet been reported for a traditional gel-electrolyte-based DSSC. In our case, the PVB-SPE film absorbs the electrolyte and remains a thin film in the solid state. The extra semicircle suggests that there is an additional interface that offers an extra resistance-capacity couple in our PVB-SPE electrolyte DSSC. In other studies, traditional PGEs, which are usually prepared by the addition of polymer powders or small molecular gelators, were formed by a thermo-reversible physical cross-linking network. The PGEs produced in this way consist of a single phase in the electrolyte and, as a result, present only one semi-circle, which indicates the diffusion ability of I_3^-/I^- in the electrolyte in the Nyquist plot [26]. However, in our case, some of the liquid electrolyte is squeezed out of PVB-SPE during the hot-pressing process of fabrication. After reacting with an oxidizing dye, the I_3^-/I^- in the liquid electrolyte will diffuse to and across the PVB-SPE film to the Pt electrode. It is reasonable to believe that there exists an extra interface (electrolyte/ PVB-SPE) that produces an additional resistance-capacity couple and therefore an extra semi-circle in the Nyquist plot.

It is also evident that type II PVB-SPE thin film (MPN+PVB)-based DSSCs exhibit only 69%

the efficiency of corresponding type II-LSE liquid cells. However, the cells based on the type I PVB-SPE thin film containing ion channels (GBL+NMP+PVB) retain a remarkable 94% of the efficiency of corresponding type I-LSE liquid cells. This result indicates that the ion channels could relieve the adverse effects of the extra interface.

3.5. Long-term stability of the GBL+NMP+PVB electrolyte DSSC

Fig. 10 shows one of the most important properties of DSSCs—the lifetime [27]. It is known that the total electricity generated by DSSCs is not limited only by the instantaneous photoelectric conversion efficiency of cells. The long-term durability of the type I PVB-SPE-based DSSC was evaluated.

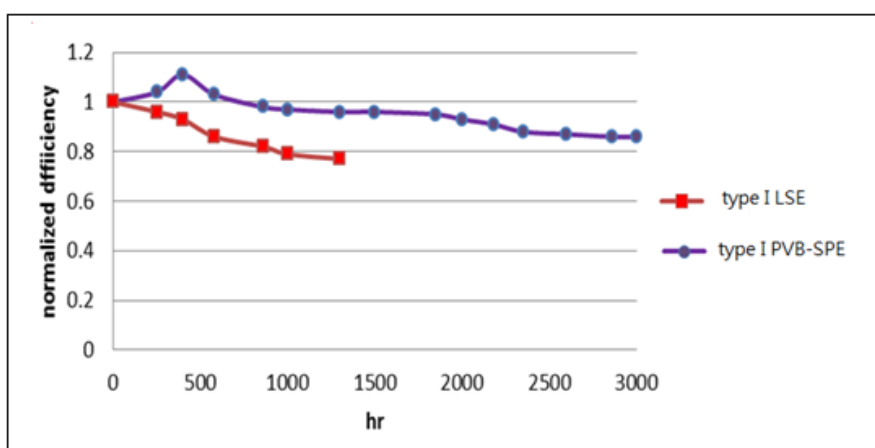


Figure 10. the long-term durability of type I LSE and PVB-SPE

It is known that

$$P = I \times V \tag{5}$$

and

$$E = I \times V \times t \tag{6}$$

where P is power throughput, E is the total energy throughput, I is current, V is voltage, and t is the duration time. It is also known that [28]

$$\eta = \frac{I_{sc} V_{oc} FF}{P_{in}} = \frac{I_{max} V_{max}}{P_{in}} \tag{7}$$

where η is the efficiency and P_{in} is the input power from sunlight or solar simulators. This

equation can be modified to read $P_{in} \times \eta = I_{max} \times V_{max}$ and substituted into equation (6). Thus, the total energy throughput is obtained as follows:

$$E = P \times \eta \times t \tag{8}$$

For comparison, the conversion efficiency as a function of time of the type I LSE (liquid electrolyte) DSSC was also determined. The lifetime is defined as the time required to reach 80% of the normalized efficiency, which is the efficiency measured at a given time divided by the efficiency measured at time zero.

The total electricity generated can be calculated by the following equation:

$$E = \int_0^{t_{life}} P_{in} \eta \cdot dt \tag{9}$$

where E is the total electricity generated by a DSSC, P_{in} is the input power from sunlight or simulated light, η is the conversion efficiency of a DSSC, and t_{life} is the lifetime of a DSSC. Normally, we assume that P_{in} remains constant throughout the measurement. As a result, the total amount of electricity generated by a DSSC depends on the product of the conversion efficiency and the DSSC lifetime.

For convenience, we could make the assumption that the two decay curves of the normalized efficiencies in Fig. 10 are two straight lines. Thus,

$$\frac{E_1}{E_2} = \frac{t_{life1} \cdot \eta_1}{t_{life2} \cdot \eta_2} = \frac{3000 \times 5.458 \times \frac{(1+0.86)}{2}}{1000 \times 5.836 \times \frac{(1+0.79)}{2}} = 2.92$$

where E_1 , t_{life1} , and η_1 represent the solid-state DSSC assembled with the type I PVB-SPE and E_2 , t_{life2} , and η_2 represent the liquid-state DSSC assembled with the type I LSE. As a result, the total amount of electricity generated by the solid-state DSSC device is 2.92 times the total amount generated by the liquid-state DSSC device. In our research, DSSC devices with long-term stability and only a slight decrease in efficiency can be reproduced.

4. CONCLUSION

PVB-SPE-based DSSCs were fabricated by placing an ion-conductive PVB thin film between a TiO_2 working electrode and a Pt counter electrode, and their photo-to-electric conversion efficiency and electrochemical properties were evaluated. The ionic conductivity of the PVB-SPE system was observed to increase with the length of time that PVB was immersed in the electrolyte. The quasi-solid-state DSSC assembled with an ion-conducting PVB-SPE thin film exhibited a high conversion efficiency of 5.46%, approximately 94% the conversion efficiency of liquid-state cells. The lifetime of

ion-PVB-based DSSCs can reach over 3000 hours, which is much better than the lifetime of liquid-state DSSCs. The results of this study suggest that ionically conductive PVB, as a quasi-solid polymeric electrolyte, is a promising material for developing practical solar cells with good, long-term stability.

References

1. B. O'Regan and M. Gratzel, *Nature*, 353 (1991) 737.
2. Tzu-Chien Wei, , Shien-Ping Feng, Ya-Huei Chang, Sheng-Jye Cherng, Yu-Jie Lin, Chih-Ming Chen and Han-Hsu Chen, *Int. J. Electrochem. Sci.*, 7 (2012) 11904.
3. Hanmin Tian, Xirui Yu, Jiuyan Zhang, Wenfeng Duan, Fenglan Tian and Tao Yu , *Int. J. Electrochem. Sci.*, 7 (2012) 4686.
4. Fan Xing, Chu Zengze, Wang Fuzhi, Zhang, Chao, Chen Lin, Tang, Yanwei and Zou Dechun, *Adv. Mater.*, 20 (2008) 592.
5. Aswani Yella, Hsuan-Wei Lee, Hoi Nok Tsao, Chenyi Yi, Aravind Kumar Chandiran, Md.Khaja Nazeeruddin, Eric Wei-Guang Diao, Chen-Yu Yeh, Shaik M Zakeeruddin and Michael Grätzel, *Science*, 334 (2011) 629.
6. Henry J Snaith, *Adv. Funct. Mater.*, 20 (2010) 13.
7. Lim Su Jung, Kang Yong Soo and Kim Dong-Won, *Electrochim. Acta*, 56 (2011) 2031.
8. A. F. Nogueira, C. Longo and M. A. De Paoli, *Coord. Chem. Rev.*, 248 (2004) 1455.
9. P. Wang, S. M. Zakeeruddin, J. E. Moser, R. H. Baker and M. Gratzel, *J. Am. Chem. Soc.*, 126 (2004) 7164.
10. K. Tennakone, V. P. S. Perera, I. R. M. Kottegoda and G. Kumara, *J. Phys. D: Appl. Phys.*, 32 (1999) 374.
11. B. O'Regan, and D. T. Schwartz, *Chem. Mater.*, 10 (1998) 1501.
12. Francisco Fabregat-Santiago, Juan Bisquert, Le Cevey, Peter Chen, Mingkui Wang, Shaik M. Zakeeruddin, and Michael Gratzel, *J. Am. Chem. Soc.*, 131 (2009) 558.
13. Francisco Fabregat-Santiago, Juan Bisquert, Emilio Palomares, Saif A. Haque, and James R. Durrant, *J. Appl. Phys.*, 100 (2006).
14. Steele BCH, and Heinzl A, *Nature*, 414 (2001) 345.
15. Antonino Salvatore Aricò, Peter Bruce, Bruno Scrosati, Jean-Marie Tarascon and Walter van Schalkwijk, *Nat. Mater.*, 4 (2005) 366.
16. J.M. Tarascon and M. Armand, *Nature*, 414 (2001) 359.
17. G.P. Kalaignan, M.S. Kang and Y.S. Kang, *Solid State Ionics*, 177 (2006) 1091.
18. Bhattacharya Bhaskar, Lee Jun Young and Geng Jianxin, *Langmuir* 25 (2009) 3276.
19. Lee Yuh-Lang, Shen Yu-Jen and Yang Yu-Min, *Nanotechnology*, 19 (2008) 455201.
20. T. C. Wei, C. C. Wan, Y. Y. Wang and *Sol. Energy Mater. Sol. Cells*, 91 (2007) 1892.
21. Hongxun Yang, Miaoliang Huang, Jihuai Wu, Zhang Lan, Sancun Hao and Jianming Lin, *Mater. Chem. Phys.*, 110 (2008) 38.
22. Park Sung-Hae, Choi Hyung-Ju, Lee Su-Bin, Lee, Seung-Min, Cho Sang-Eun, Kim Ki-Hyun, Kim Young-Keun Kim Mi-Ra and Lee Jin-Kook, *Macromol. Res.*, 19 (2011) 142.
23. Hitek Glass, No.789 Bo-Ai street, Chu Bei, Taiwan, 886-3-6561277.
24. Mingxing Wu, Yudi Wang, Xiao Lin, Naisen Yu, Liang Wang, Linlin Wang, Anders Hagfeldt and Tingli Ma, *Phys. Chem. Chem. Phys.*, 13 (2011) 19298.
25. M. K. Nazeeruddin, A. Kay, I. Rodicio, R. Humphry-Baker, E. Mueller, P. Liska, N. Vlachopoulos and M. Graetzel, *J. Am. Chem. Soc.*, (1993) 6382.
26. Motornari Adachi, Masaru Sakamoto, Jinting Jiu and Yukio Ogata, Seiji Isoda, *J. Phys. Chem. B*, 110 (2006) 13872.

27. Guogang Xue, Yong Guo, Tao Yu, Jie Guan, Xirui Yu, Jiyuan Zhong, Jianguo Liu and Zhigang Zou, *Int. J. Electrochem. Sci.*, 7 (2012) 1496.
28. Jenny Nelson, Imperial College Press, London, 2002.